Article published online: 2021-01-18

Organic Materials C.-W. Chu, C. A. Schalley THIEME OPEN ACCESS Review

Recent Advances on Supramolecular Gels: From Stimuli-Responsive Gels to Co-Assembled and Self-Sorted Systems

Chih-Wei Chu[a]
Christoph A. Schalley*[a]

[a] Institut für Chemie und Biochemie, Freie Universität Berlin, Arnimallee 20, 14195 Berlin, Germany
c.schalley@schalley-lab.de

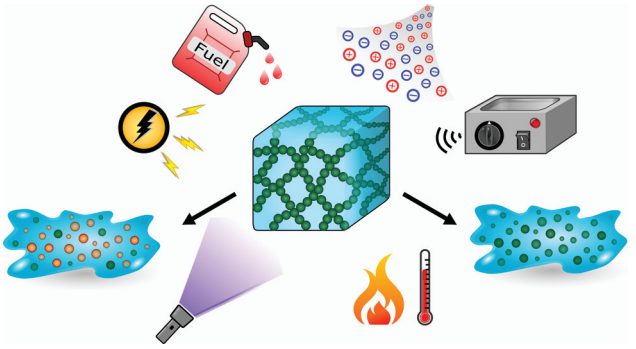

Received: 31.10.2020
Accepted after revision: 04.12.2020
DOI: 10.1055/s-0040-1722263; Art ID: om-2020-10-0039rev

Abstract Gels prepared from low-molecular-weight gelators (LMWGs) represent versatile soft materials. Self-assembly of LMWGs forms nanofibers and above critical gelation concentrations, the entanglement of which leads to self-supporting gels. Owing to the dynamic properties of the self-assembly process, stimuli-responsive LMWGs have prospered in the last decade. In addition, incorporating multiple LMWGs into one system brings the opportunity to achieve sophisticated designs and functions. This review covers recent advances in the field of supramolecular gels, from stimuli-responsive gelators to multicomponent systems that are self-sorting and/or co-assembling.

Key words low-molecular-weight gelators, supramolecular polymers, stimuli-responsive systems, dissipative systems, self-sorting, co-assembling

Introduction

A supramolecular gel, in general, is defined as a gel that utilizes noncovalent interactions to form three-dimensional entangled networks in a given solvent.[1,2] Depending on the backbone of the networks, they can be further classified as polymeric or molecular gels. Supramolecular polymeric gels, self-explaining from the term, are constructed with polymers as backbones and additional noncovalent interactions to increase the number of cross-linking points (Figure 1a). Classic interactions include host–guest (e.g. crown ether-,[3,4] cyclodextrin-,[5,6] and cucurbituril-based[7,8] systems) and ionic interactions.[9,10] In contrast to polymeric gels, the backbones of molecular gels are indeed self-assembled from low-molecular-weight gelators (LMWGs) through noncovalent interactions (Figure 1b), such as hydrogen bonding, π–π, and metal–ligand interactions.

The gelation of LMWGs is highly dynamic. The gelators are first dissolved in a "highly soluble" state, such as at a higher temperature or in a good solvent. When, for example, a decreased temperature brings them to a "poorly soluble" state, the hierarchical self-assembly of a supramolecular gel occurs. The gelators nucleate and self-assemble along one dimension forming nanofibrils, which frequently form fibril bundles. When the nanofibers reach a certain length, they entangle into the gel network in which the solvent is trapped. During gelation, the self-assembly of LMWGs is most likely a kinetic trapping process and the mechanical properties of the gels often depend on the exact conditions of the self-assembly process.[11,12]

Starting already in the late 1990s, efforts have been invested in both discovering new LMWGs and understanding their gelation[13–16] and the properties of the supramolecular materials based on them.[17,18] Owing to their dynamic

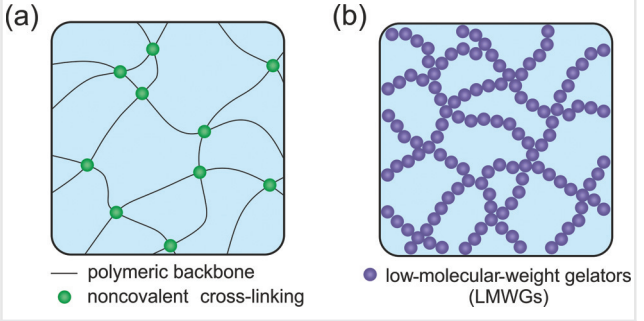

Figure 1 Schematic representation of (a) supramolecular polymeric gels and (b) gels made by LMWGs.

Biosketch

Christoph Schalley studied chemistry at the University of Freiburg, Germany and graduated in 1993 from the Technical University Berlin. In his Ph. D. work with Helmut Schwarz at TU Berlin, he received his thorough education as a mass spectrometrist and gas-phase chemist. After postdoctoral work on supramolecular chemistry with Julius Rebek, Jr. at The Scripps Research Institute, La Jolla, United States, he combined both topics when he started his own research group as a habilitand at the University of Bonn. In 2005, he was appointed professor of organic chemistry at Free University Berlin. Meanwhile, Schalley and his group's research topics are diverse and comprise supramolecular chemistry in the gas phase as well as in solution and at interfaces.

Chih-Wei Chu studied chemistry and obtained his bachelor and master's degrees in Taiwan before he moved to Germany. In 2015, he became a Marie-Curie Fellow and took an MSCA-ITN-funded position to pursue his doctoral degree under the supervision of Prof. Dr. Bart Jan Ravoo at WWU Münster. In July 2018, he defended his doctoral thesis, focusing on stimuli-responsive soft materials. Starting from December 2018, he is a postdoctoral researcher in the group of Prof. Dr. Christoph Schalley at Freie Universität Berlin. His research interests include supramolecular gels, light-responsive (pseudo)rotaxanes, and molecular switches.

properties, LMWGs can respond to various stimuli. Several overviews of stimuli-responsive LMWGs, involving pH,[19,20] metal as well as organic ions,[21,22] and physical stimuli,[23,24] have been published. In addition, to expand the functions and applications of supramolecular gels, implementation of multiple LMWGs into a system is underway.[25,26]

In this review, we highlight recent progresses in stimuli-responsive gels and multicomponent systems in the last decade. To give the readers a different perspective, in the sections of responsive gels, the stimuli are discussed in two ways: stimuli that (1) cause changes to the environment and indirectly affect the gel or (2) induce changes in the gelators themselves. In the sections of multicomponent systems, self-sorting and co-assembling of LMWGs, and the process to control, these two systems will be explored.

Stimuli-Induced Changes in the Environment

Some stimuli affect the environment, so that they indirectly alter the self-assembly of LMWGs, leading to sol–gel or gel–sol transitions. Three stimuli, ions, heat, and ultrasound, are taken as examples in this section.

Ions

LMWGs are often sensitive to ions, both in organo- and hydrogels. Recently, Steed and coworkers reported a metal-ion- and anion-responsive organogelator based on pyridinylmethyl urea **1** (Scheme 1).[27] This gelator forms a strong gel in aromatic solvents ($G' = 20–70$ kPa at low stress) due to an α-tape hydrogen-bonded motif between the urea groups. When inorganic salts are introduced, the gel is weakened or even destroyed. On one hand, metal ions such

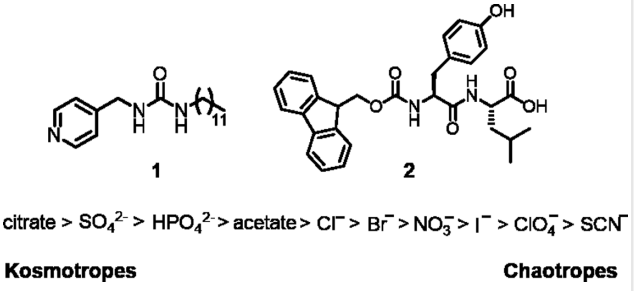

Scheme 1 Molecular structures of gelators that respond to ions and Hofmeister series.

as Cu^{2+} and Zn^{2+} coordinate the pyridinyl nitrogen atoms in **1**, disrupting its self-assembled structure. On the other hand, the corresponding anions, for example Cl^- may bind to the urea groups through quite strong hydrogen bonds.[28,29] This then leads to the collapse of the urea α-tape motif, hence the gel is weakened. The rheological data reveal that the metallogels are softer as they exhibit an elastic modulus lower by at least one order of magnitude compared to **1** alone. When $Co(NO_3)_2$ is added to **1** in nitrobenzene, the gel is completely destroyed as the octahedral complex $[Co(\mathbf{1})_2(NO_3)_2(\text{nitrobenzene})_2]$ does not form a supramolecular gel. Surprisingly, its sol–gel transition could be triggered after a certain amount of tetrabutylammonium bromide (TBABr) was added. The addition of a minimum of 0.3 equivalent of TBABr leads to tetrahedrally coordinated $[Co(\mathbf{1})_2Br_2]$ complexes that are able to form gels again.

In contrast to organic media, electrolytes have rather subtle effects on gelators in aqueous solution. Yet, they are known to have indirect control over the self-assembly by influencing the structure of water. The strength of the electrolytes is ordered by the so-called Hofmeister series (Scheme 1). This effect has been studied not only in protein folding,[30] but also in polymeric systems.[31] Ulijn and coworkers reported a systematic study of specific ion effects on the gelation of an aromatic dipeptide amphiphile **2** (Scheme 1).[32] Self-assembly of hydrogelator **2** is a result of combined interactions of π–π stacking between Fmoc moieties and hydrogen bonding between the amide groups, which form a β-sheet structure. Although **2** is anionic at pH 8, it can self-assemble when 100 mM of salt is added due to the shielding of repulsive electrostatic interactions. Both circular dichroism (CD) and rheology reveal that the self-assembly of **2** is influenced significantly by anions and the effects follow the Hofmeister series. In the presence of kosmotropic ions such as citrate, sulfate, and phosphate, an intense positive signal between 260 and 300 nm in the CD spectra is observed, suggesting the formation of helical fibers with a strong preference for one helicity. This is because that kosmotropes can promote the interactions between water molecules, so that hydrophobic interactions in self-assembled **2** are significantly enhanced. Usually, when the gelators have a preferred helicity for stacking, their hierarchical self-assembly may result in a more densely packed structure, thus influencing the macroscopic outcomes, such as rheology. The same trend is observed by rheology: Stiffer materials ($G' > 2{,}000$ Pa) are found when kosmotropes are added. Instead, in the presence of chaotropic ions, such as perchlorate and thiocyanate, not only the positive signal in CD is largely reduced, but a softer material ($G' < 1{,}000$ Pa) is detected in rheology at the same conditions.

Heat

Usually, gelation of LMWGs goes through an annealing process, because most gelators are better solvated at high temperatures and start to aggregate upon slow cooling. Moreover, the mechanical properties of the gel such as rheology are often dependent on its heating–cooling process.[33,34] There are, however, some rare cases,[35] in which they show a reverse trend. These are so-called heat-set gelators that self-assemble at higher temperatures. Some of the heat-set gelators have a similar effect on polymers with lower critical solution temperature, i.e. noncovalent interactions between the gelators are enhanced by releasing solvent molecules from their solvation shell into the bulk solution at higher temperature.

An early example of heat-set metallogelator was reported in 2004, in which a change in coordination geometry occurred upon heating.[36] Nitschke and coworkers investigated metallopolymers that increased the number of cross-linking points when the temperature was elevated.[37] The imine chelate ligand was synthesized via the condensation of 1,4-phenylenediamine and bispyridine dicarbaldehyde. In the presence of trioctylphosphine as additional ligands to the vacant coordination sites of copper(I), the linear metallopolymers **3** were obtained (Figure 2). At room temperature, the linear, non-cross-linked metallopolymers are expected based on the observation that heteroleptic species $[CuN_2P_2]^+$ are favored compared to homoleptic complexes $[CuN_4]^+$. Although the ligand exchange of two $[CuN_2P_2]^+$ to give $[CuN_4]^+$ and $[CuP_4]^+$ between two metallopolymer chains is enthalpically unfavorable, it becomes progressively desirable as the entropy increases at higher temperature. The increasing number of $[CuN_4]^+$ cross-links eventually brings the system to a gel state. The ligand exchange at higher temperature comes along with changes in color (from orange to green) and intensity of both absorption and emission, so that one could monitor the process not only macroscopically but also spectroscopically. This principle is later applied by the same group to develop a light-emitting electrochemical cell.[38]

In 2014, Miravet and coworkers reported bolaamphiphilic hydrogelator **4**, which is based on an L-valine derivative (Figure 3).[39] Self-assembly of this gelator is driven by the hydrophobic effect with complementary interactions of hydrogen bonding and π–π interactions. When a chaotropic ion is present, the individual gelator is better stabilized and, thus, the solubility is enhanced. Interestingly, when the guanidinium ion is incorporated as an additive, the resulting gel shows a heat-set effect. It was reported that guanidinium cations are capable of forming hydrogen bonds with both amide and urea groups.[40] NMR spectroscopy reveals a constant solubility (9 mM) of **4** in

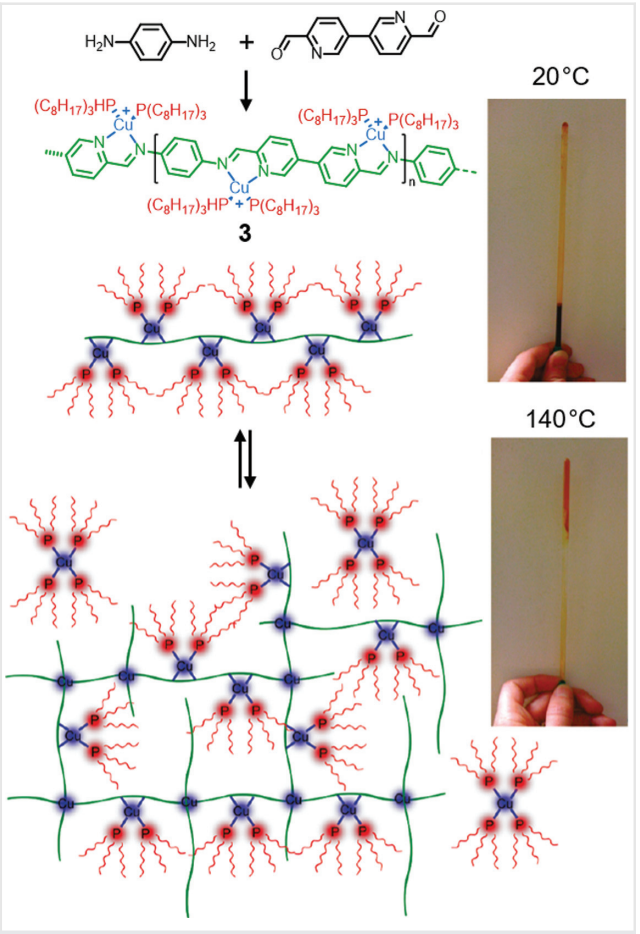

Figure 2 Synthesis of metallopolymers **3** and their thermal response. Adapted with permission from Ref. 37. Copyright 2011 American Chemical Society.

pure water below 55 °C. In the presence of guanidinium ions, the solubility of the gelator shows a clear temperature dependence and decreases from 35 °C (>13 mM) to 55 °C (9 mM) because of the weakening of the guanidinium/**4** hydrogen bonds upon heating. As a consequence, the release of guanidinium cation initiates the self-assembly of **4** at higher temperatures and a gel forms. Rheological measurements agree with this interpretation. At room temperature **4** is fully dissolved ($G'' > G'$) and upon heating above 40 °C, a viscoelastic material ($G' > G''$) is obtained. Surprisingly, the hydrogel does not collapse immediately when the sample is cooled back down. This suggests the hydrogel to be metastable with slow disassembly kinetics at room temperature. Indeed, this heat-treated, self-supported gel remained stable at room temperature for at least 48 hours. In the given example, gelation of **4** is not solely controlled by heat but shows dependence on the presented ions, underlying the complexity of the gelation of LMWGs.

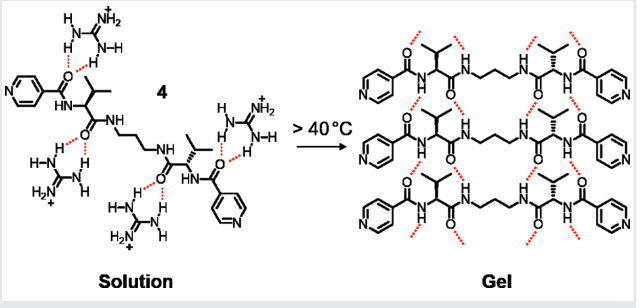

Figure 3 Heat-triggered gelation of **4** by releasing guanidinium ions above 40 °C.

Ultrasound

Ultrasound produces mechanical waves with high frequency (>20 kHz) and causes the so-called cavitation effect. Cavitation describes the phenomenon that microbubbles nucleate, propagate, and collapse in the liquid. When the microbubbles collapse, mechanical stress is generated. This effect has been widely utilized in daily life, such as in cleaning and in homogenizing heterophases. More importantly, it has also been proven to promote reactivity and selectivity in organic synthesis, i.e. sonochemistry.[41,42] Such pressure waves may assist in overcoming energy barriers and disturbing intermolecular interactions, so that self-assembly of LMWGs can be brought to a(n) (another) metastable state and the gelation processes can be controlled. The term sonogelator was coined to describe those molecules that form gels under ultrasound irradiation.[43]

The first sonogelator was reported as early as 2005.[44,45] Chiral macrocycles **5** with clothespin-shaped structures were prepared from *trans*-bis(salicylaldiminato) metal complexes, which were doubly linked with pentamethylene groups in the *anti*-conformation.[44,46] In 2015, Naota and coworkers demonstrated the formation of heterometallic arrays by mixing Pd- (**5a**) and Pt-centered (**5b**) complexes (Figure 4a).[46] Both the Pd and Pt complexes show heterochiral aggregation, meaning that the arrays assemble with alternating chirality regardless of the metal center. The heterochiral aggregation is attributed to the balance of inter- and intramolecular π–π stacking as well as intermolecular metal–metal interactions. In the Pt-enriched systems (**5b**:**5a** > 2:1), gelation takes place within 1 hour at ambient temperature without sonication, whereas the Pd-dominated systems (**5a**:**5b** > 2:1) require additional ultrasonic energy to form gels. This observation can be rationalized by the inherent differences in molecular structure. Complex **5a** has an A-shaped conformation because of the weak π–d conjugation around the Pd core and the intramolecular π-stacking, which bend the *trans*-bis(salicylaldiminato)Pd blades (Figure 4b). In contrast, the

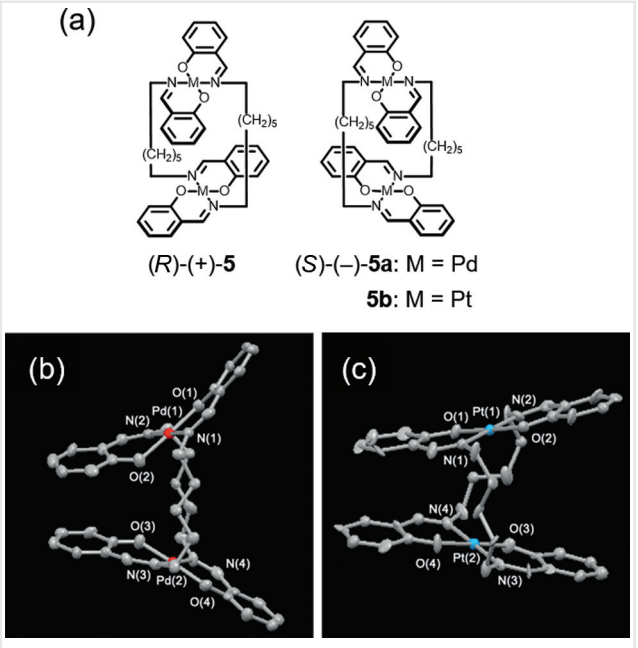

Figure 4 (a) Molecular structures of sonogelators **5a** and **5b**. Conformations of (b) the A-shaped Pd complex (*R*)-**5a** and (c) the H-shaped Pt complex (*S*)-**5b**. Adapted with permission from Ref. 46. Copyright 2015 John Wiley &Sons.

stronger π–d conjugation around the Pt core and thus the more rigid coordination platforms make **5b** an H-shaped complex (Figure 4c). In the solution state, both **5a** and **5b** form spherical aggregates (stable state for **5a**; metastable state for **5b**). In the metastable Pt-enriched particles, the H-shaped units grow as seeds and these propagate through intermolecular interactions to form nanofibrils. On the contrary, the stable Pd-enriched colloids bear A-shaped units with stronger intramolecular π–π interactions at their surfaces, which prevents the spontaneous interpenetrating stacking association. Upon sonication, some of the A-shaped units transform into H-shaped structures. This leads to the generation of seeding sonocrystals, and subsequently to the formation of longer fibers.

Apart from metallogels, sonogelators based on pure organic components are commonly observed for cholesterol, urea, and amide derivatives.[47] For instance, Ulijn and coworkers utilized ultrasound to control the self-assembly of peptides, align these nanostructures, and finally influence the gelation.[48,49] Recently, Hunter and coworkers reported a macrocycle **6** that gelates upon sonication.[50] In the solution state, a kinetically trapped conformation of **6** is present due to the *intra*molecular π–π stacking between the terephthalate and hydroquinone moieties (Figure 5). With the assistance of ultrasonic energy, the activation barrier associated with the unfolding of this conformation could be

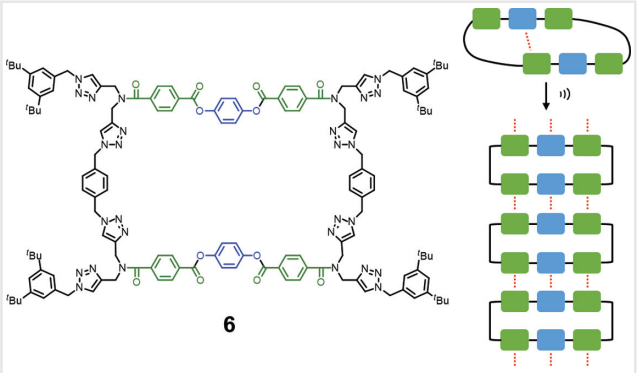

Figure 5 Molecular structure of sonogelator **6** and the proposed mechanism for the self-assembly of **6** under ultrasound. Adapted with permission from Ref. 50. Copyright 2018 The Royal Society of Chemistry.

overcome.[23] As a result, the *intra*molecular aromatic interactions in **6** are cleaved, thus allowing extended *inter*molecular aromatic interactions to form nanofibrous assemblies.

Stimuli-Induced Changes in the Gelator Molecules

There are other stimuli, which cause changes in the structure of the gelator and thus affect its gelation ability. In this section, three stimuli, i.e. redox processes, light irradiation, and chemical reactions, are highlighted.

Redox Processes

Redox active gelators have been controlled by chemical or electrochemical oxidation, so that temporal control could be achieved.[51]

Ferrocene (Fc) not only has fully reversible electrochemical properties, but is also stable in aqueous media. These properties make it a popular candidate for biological and sensory applications.[52,53] In the neutral state, Fc is a hydrophobic and neutral molecule, whereas upon oxidation, the ferrocenium (Fc^+) becomes hydrophilic and ionic. Kraatz and coworkers demonstrated that a ferrocene-conjugated amyloid tripeptide **7** (Figure 6) gelates in toluene with the assistance of heating and ultrasound.[54] After adding $Fe(ClO_4)_3$ as the oxidant, the Fc^+ derivative is produced and a gel–sol transition is triggered accompanied by a visible color change. Spectroscopically, the Fc-peptide exhibits a reversible absorbance at 446 nm in the UV-Vis spectrum, and a positive CD signal at 504 nm, indicating the helical fibers formed due to the self-assembly. As for the oxidized Fc^+-peptide, the absorbance in the UV-Vis spectrum is shifted to 636 nm, and the signature of the

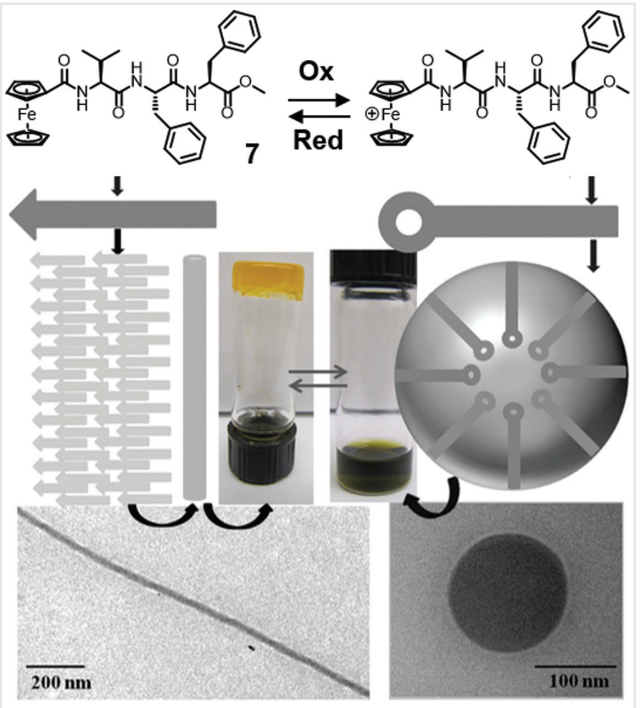

Figure 6 Redox active gelator **7** (top) with different modes of assembly. β-Sheet-like structure for neutral **7** (bottom left) and micelle-like spherical structure for oxidized **7** (bottom right). Adapted with permission from Ref. 54. Copyright 2014 The Royal Society of Chemistry.

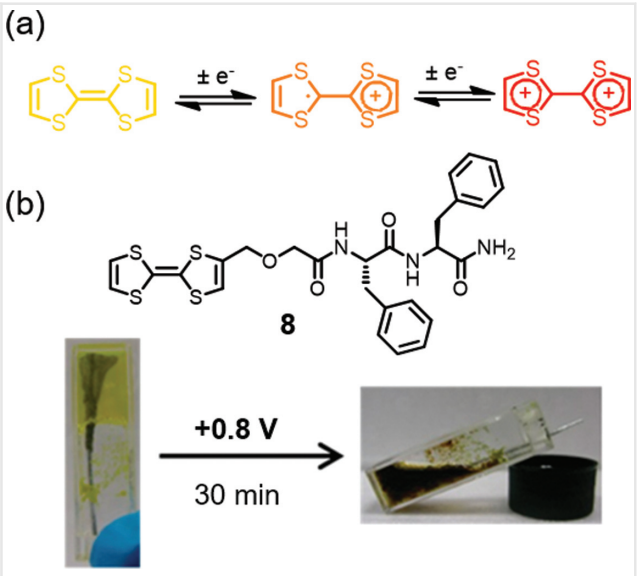

Figure 7 (a) Stepwise oxidation of TTF. (b) Redox active gelator **8** and the sol–gel transition upon electrochemical oxidation. Adapted with permission from Ref. 57. Copyright 2014 American Chemical Society.

helical fibers in the CD spectrum is diminished. More interestingly, transmission electron microscopy (TEM) images reveal the self-assembled structures of Fc- and Fc^+-peptide. The entangled fibrous structures are indeed observed in the case of the Fc-peptide, whereas micelle-like spheres are found for the Fc^+-peptide. This significant difference is due to the ionic Fc^+ groups, which tend to aggregate to minimize their interactions with the hydrophobic solvent.

Tetrathiafulvalene (TTF) is a redox-active organosulfur compound. Its oxidation occurs in two steps: first, to a radical-cation state, then further to a dication (Figure 7a). TTF has found its place in organic electronics applications[55] and as a redox motif in mechanically interlocked molecules.[56] Nalluri et al. discovered that a TTF-appended organogelator (**8**) forms conductive nanofibers upon doping with tetracyanoquinodimethane (TCNQ).[57] The organogel of **8** in chloroform forms within 30 minutes and is stable for months. This is a result of the balance between intermolecular π–π stacking of TTF motifs and the hydrogen bonding of diphenylalanine peptides. Upon oxidation, either chemically (addition of $NOPF_6$) or electrochemically (applying +0.8 V), a brownish precipitate forms, and the gel breaks down (Figure 7b). Notably, the gel state persists with a brownish color when 1 equivalent of TCNQ is added. Rheology even suggests that — instead of disturbing the self-assembly of **8** — doping with TCNQ indeed enhances the gel's stiffness. Also, the strongly altered color is an indicator of the formation of a charge transfer complex ($TTF^+/TCNQ^-$). These observations reveal the TCNQ to intercalate between the TTF units of **8** in the self-assembled state thus forming a more densely packed and entangled nanofibrous network. The conductivity of the gel increases from 1.9×10^{-10} (pure **8**) to 3.6×10^{-4} S cm^{-1} (doped with TCNQ).

Light Irradiation

Using light as a stimulus in supramolecular gels is of great interest. Light is not only a noninvasive stimulus, but it also provides a high spatial and temporal resolution. Well-studied light-responsive functional groups can be categorized by the processes induced upon irradiation: isomerizations (e.g., azobenzenes), ring-closing/opening reactions (e.g., spiropyrans and diarylethenes), cycloadditions (e.g., anthracene and coumarin dimers), polymerization (e.g., diacetylenes), and through photocleavages (e.g. cleavage of a 2-nitrobenzyl group).[24] In this section, three classes of light-responsive groups including photoisomerizations, ring--closing/opening reactions, and molecular motor-like rotations are exemplarily discussed.

Speaking of photoinduced configurational isomerization, azobenzene is no doubt an iconic example in this

category. Taking such a dramatic change in polarity between the *E*- and the *Z*-isomer as an advantage; the first light-responsive organogel was reported more than 25 years ago.[58] Hughes and coworkers investigated azobenzene-appended organogelator **9**, which bears a photoresponsive unit and a benzoyl chloride moiety to enable facile functionalization (Scheme 2a).[59] Upon exposure to light, changes in properties are not only investigated at the molecular level but also visualized macroscopically. It is especially interesting to see the in situ transformation between gel and solution under light irradiation in such highly ordered self-assemblies. Both in situ photorheology and real-time synchrotron small-angle X-ray scattering (SAXS) were carried out. Rheological measurements reveal *E*-**9** to form a stable gel ($G' > G''$) with a storage modulus of about 1,000 Pa. As soon as UV light is switched on, both moduli dramatically drop and G' and G'' become closer to each other (both moduli < 100 Pa). A new plateau is reached within 1 minute. The corresponding change in viscosity is also observed, i.e., a low viscosity fluid is obtained upon UV irradiation. After visible light irradiation, its viscosity is restored close to the initial state within a couple of minutes. In good agreement, diffraction peaks indicative of fiber aggregation are observed in SAXS measurements only for *E*-**9**. Multiple light switching cycles can be done. Recent strides using azobenzene to obtain light-switchable gels also include incorporating azobenzene as a hydrophobic moiety in peptide amphiphiles with different amino acid sequences.[60,61]

In the ring-opening/closing category, diarylethene may serve as an example here. Unlike to photoisomerizing groups, this photoswitch does not exhibit large changes in molecular geometry upon irradiation. Instead, the open and closed diarylethenes differ in conjugation, making it a photochromic switch. Owing to the thermal stability of both the open and the closed form in the dark, diarylethenes have been applied as optical memories and switches.[62,63] In 2014, van Herpt et al. reported a series of hydrogelators, in which the open form of a maleimide-based dithienyl switch is coupled to various dipeptides (Scheme 2b).[64] The self-assembled structures of hydrogelator **10** and its analogues were studied by traditional TEM and cryo-TEM, and interestingly, they all showed similar curled sheet-like structures. This indicates the dipeptides to act as solubilizing groups and the photoswitch to be the core motif for the self-assembled structure. Upon irradiation at 312 nm, the photocyclization takes place from open-**10** to close-**10** along with the corresponding extension of the conjugated π-system. This results in a color change from yellow (open-**10**) to red (closed-**10**) due to the difference in the HOMO/LUMO band gap. The photocyclization can be reversed using visible light (>500 nm) and the switching was performed for multiple cycles. Although the photochromic effect is distinctive, no changes in rheological properties were observed. Because of the gel stability of both open-**10** and closed-**10** and their enormous difference in color, positive and negative photopatterning is possible and rewritable information storage can be achieved.

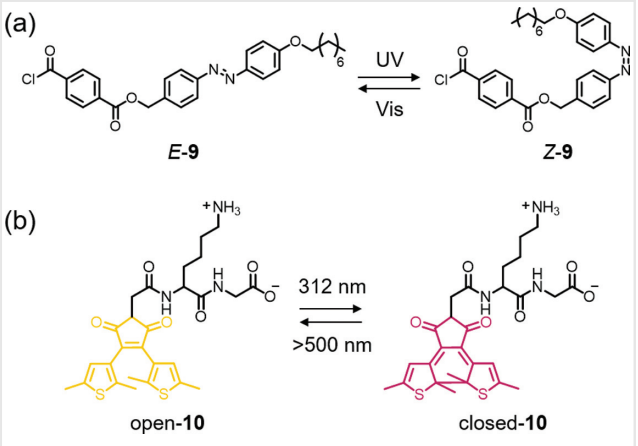

Scheme 2 (a) Light-responsive gelator **9** and the *E*- to *Z*-isomerization upon UV and visible light irradiation. (b) Light-responsive gelator **10** and the ring-closing/opening upon light irradiation.

As a last example in this subsection, we would like to focus on a molecular motor. Unidirectional molecular motors were investigated in systems triggered either by chemical reaction[65] or light.[66,67] In both, molecular chirality plays an essential role to induce unidirectional rotation. Recently, Feringa and coworkers designed an amphiphilic molecular motor **11** by adding a dodecyl chain at one end and two carboxylic acids for enhanced water solubility at the other end (Figure 8a).[68] With a methyl group at the stereogenic center in a pseudo-axial orientation, the molecular motor rotates under UV irradiation due to the photochemical isomerization of the central C = C double bond. This results in a strained isomer, because the methyl substituent is forced to adopt an energetically unfavorable pseudo-equatorial orientation. The strained isomer then undergoes a thermal helix inversion step in order to release the steric strain. In the end, the more favorable starting state is reached again. When an aqueous solution of **11** is pipetted into a Ca^{2+}-containing solution, a string with unidirectionally aligned nanofibril bundles with a minimum of 5wt% of **11** is formed due to local dehydration of the molecular motor amphiphile and the interactions between calcium ions and carboxylates. The assemblies formed by motor **11** perform a remarkably fast photoactuation compared to polymeric hydrogels.[69] The string bends towards the incoming UV light due to the rotation of the molecular motors incorporated in the nanofiber bundles (Figure 8b). X-ray diffraction experiments reveal an increase of the diameter of the nanofibers upon irradiation and the transition from unstrained-**11** to strained-**11**. This means, when assuming the total volume of the string remains

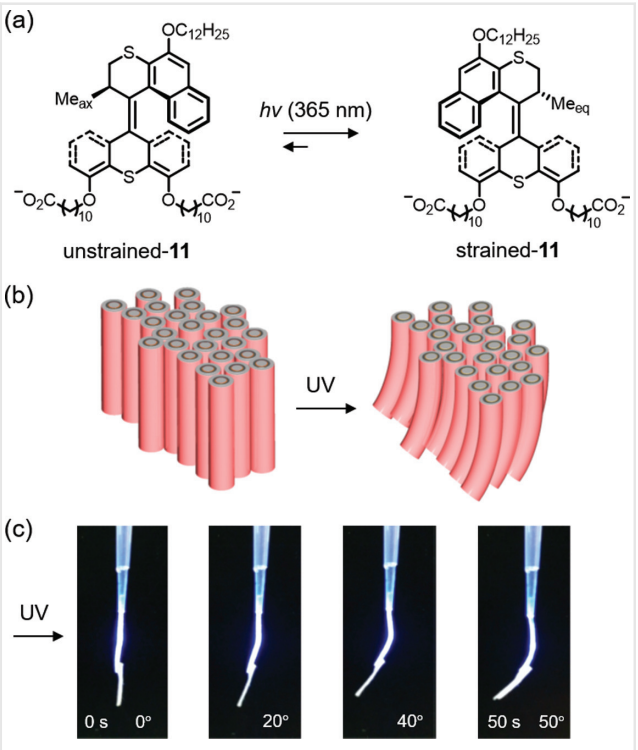

Figure 8 (a) Molecular structure and photoisomerization of molecular motor **11**. (b) Schematic representation of nanofibril bundle assembled by **11**. The nanofiber showed photoactuation and bent towards UV irradiation. (c) Photographs of weight lifting (0.4 mg) by a string of **11** upon UV irradiation. Adapted with permission from Ref. 68. Copyright 2018 Nature Publishing Group.

unchanged, the long axis should contract. Irradiation from different sides along the string leads to a zig-zag shape suggesting local and directional motion. Last but not least, it was also shown that the string had sufficient power to lift a small weight (Figure 8c).

Chemical Reactions

In recent years, supramolecular materials incorporating dissipative self-assembly have become an emerging research field.[70,71] Among them, implementing chemical fuels in the supramolecular materials provides a (spatio-) temporal control. In this subsection, three scenarios of using enzymes to either (i) adjust pH or (ii) promote peptide bond cleavage, and employing (iii) chemical reactions, such as methylation, are introduced.

Aromatic peptide amphiphiles represent a diverse class of pH-sensitive hydrogelators.[19] Compared to the traditional pH tuning by either direct acid/base addition or hydrolysis of glucono-δ-lactone (GdL),[72] treatment with enzymes such as urease and esterase unlocks the possibility of autonomous pH adjustment. Walther and coworkers presented the temporal programmability on the hydrogel of Fmoc-dipeptide **12** in the presence of urease (Scheme 3).[73] Fmoc-Leu-Gly is first dissolved at high pH (nongelator, solution state). Then, the reactants (both activator and dormant deactivator) are simultaneously added to the solution. Since the citric acid buffer (activator) leads to a rapid and drastic pH decrease, self-assembly of Fmoc-Leu-Gly takes place and the gel forms ($G' > 1{,}000$ Pa) within 1 minute. The urea (dormant deactivator) is slowly activated by urease, producing NH_3 and CO_2. Thus, after some time the original high-pH state is restored, leading to a solution ($G'' > G'$, both moduli <1 Pa). The lifetime of the gel is programmed by manipulating the concentrations of buffer, urea, and urease. In addition, when an excess of urea is added, it enables multiple cycles of pH regulation by reinjection of citric acid buffer. In another system, the use of urease is recently coupled to an amine-terminated amphiphile, in which the role of urease is reversed, i.e., the produced NH_3 initiates the self-assembly.[74]

Another example of using enzymes to transiently control gel formation was demonstrated by Ulijn and coworkers.[75,76] In this study, the same enzyme, α-chymotrypsin, is coupled to both the activation and deactivation of the self-assembly process (Scheme 4).[76] α-Chymotrypsin is known to not only catalyze peptide formation from a peptide ester (in this case, aspartame),[77] but it also catalyzes peptide hydrolysis.[78] As both reactions are catalyzed by the same enzyme, the relative rates of the activation and deactivation processes are crucial. In the beginning, when aspartame is abundant, enzyme-catalyzed formation of peptide **13** is dominant and followed by gel formation. When the fuel is more or less consumed, the enzyme-catalyzed peptide hydrolysis takes over and thus the gel breaks down. Several repetitive cycles are possible, when aspartame is refueled. Furthermore, the kinetics of gel formation and destruction can be regulated by the choice of the amino acid to be

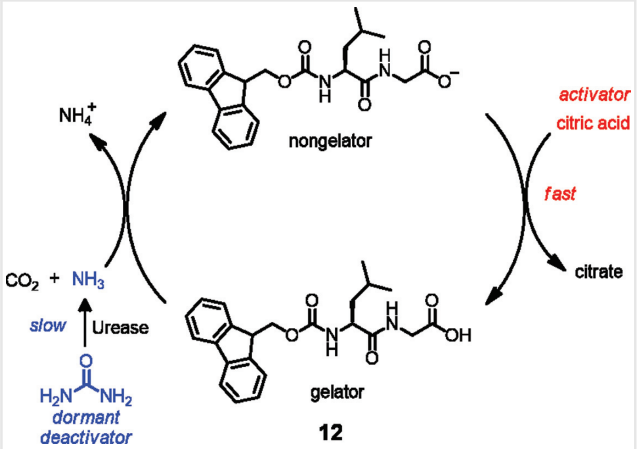

Scheme 3 Reaction cycle of enzyme-catalyzed dissipative assembly of **12**.

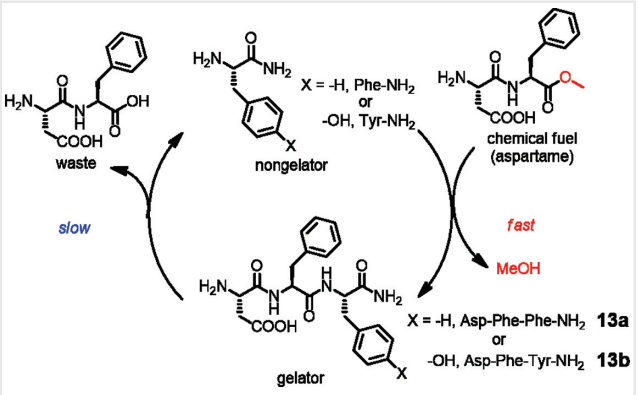

Scheme 4 Reaction cycle of fuel-driven dissipative assembly of **13**, in which α-chymotrypsin catalyzed a fast ester hydrolysis and a slow peptide hydrolysis.

coupled with the aspartame (Phe vs. Tyr). In the case of Phe-NH_2, it takes over 20 hours to accomplish one cycle, though the highest gelator concentration (**13a**) is observed already after around 30 minutes. On the contrary, in the case of Tyr-NH_2, the lifetime of the gel (**13b**) is reduced to 4 hours. The vast difference in lifetime of the two gels may be attributed to nanofiber stability differences that resulted in different hydrolysis rates.

Instead of using enzymes, Boekhoven et al. employed a chemical reaction to a dicarboxylate precursor (Scheme 5).[79,80] An alkylation reagent, either methyl iodide or dimethyl sulfate, is added to methylate the nongelating dicarboxylate. Methylated precursor **14** exhibits reduced Coulomb repulsion, leading to self-assembly of fibers and gel formation. It shows a slow activation with the relatively soft electrophile methyl iodide (over 72 hours). The somewhat harder electrophile dimethyl sulfate matches better to the dicarboxylate in terms of the hard and soft acids and bases (HSAB) principle and a gel could be obtained within 1 hour. The lifetime of the gel was determined by the rate of hydrolysis. At a pH of 11, the hydrolysis was the fastest and a solution was obtained within hours; instead, at a lower pH of 9, the gel was stable over 1 week. In addition, increasing the fuel concentration at a pH of 11 gives rise to gelator formation, thus, it elongates the lifetime of the gel. Repeating cycles can be achieved by adding new batches of fuel. Other examples of using nonenzymatic catalysis to control gel formation, e.g., hydrazone formation, have been demonstrated by van Esch, Eelkema, and coworkers.[81–84]

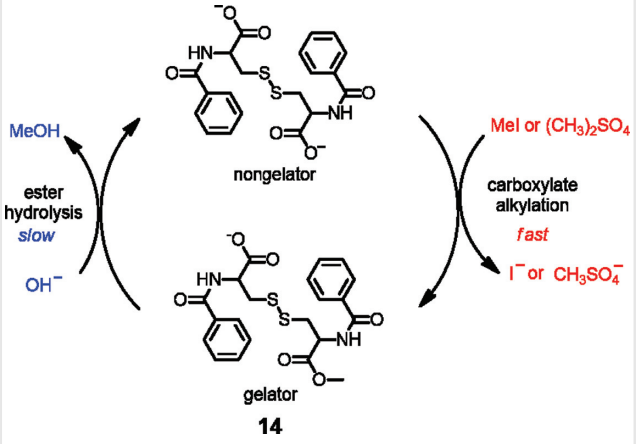

Scheme 5 Reaction cycle of dissipative assembly of **14** by taking the advantage of fast carboxylate alkylation and slow ester hydrolysis.

Multistimuli Systems

Considering systems with an activator and a deactivator immediately raises the question, how far one can push multistimuli responsiveness in LMWG systems. Indeed, some of the examples described above are actually multistimuli responsive.[39,59] Implementing multiple stimuli into LMWGs opens the door to more sophisticated systems with more complex emergent properties.

For instance, we investigated the implementation of molecular logic gates based on sol–gel transitions of a benzo-21-crown-7-functionalized bis(urea) organogelator (**15**).[85] The antiparallel arrangement of the urea groups is crucial for gelation. In addition, the tilted phenyl groups maximize the phenyl–phenyl stacking, resulting in the hierarchical self-assembly of helical fibrils and fiber bundles. The crown ethers provide additional van der Waals interactions to stabilize the assembly. In gelator **15**, there are two responsive sites, namely, the crown ethers and the urea groups. On one hand, benzo-21-crown-7 recognizes not only metal ions, such as K^+ or Ag^+, but also secondary ammonium cations (GA), with which pseudorotaxanes form. Both metal and ammonium ions bind to **15** and lead to the disruption of the gel. On the other hand, the urea–urea hydrogen bonding was significantly diminished upon addition of tetraethylammonium chloride (NEt_4Cl), since chloride ion was an effective binder for the urea group. All stimuli can be reversed to restore the gel: potassium ions can be removed by adding [2.2.2]cryptand that competes with **15** to capture potassium ions. The pseudorotaxanes dissociate, when the ammonium ions are deprotonated with a base. The chloride, finally, can be precipitated by adding KPF_6 or $AgPF_6$. Hence, the urea groups are again available for urea–urea hydrogen bonding. By precise programming with the above stimuli, a total of seven different logic gates could be realized, e.g., the OR, AND, and XOR gates, exemplarily shown in Figure 9.

In the above example, the multiple stimuli, by which the sol–gel transitions are caused, do not change the structure

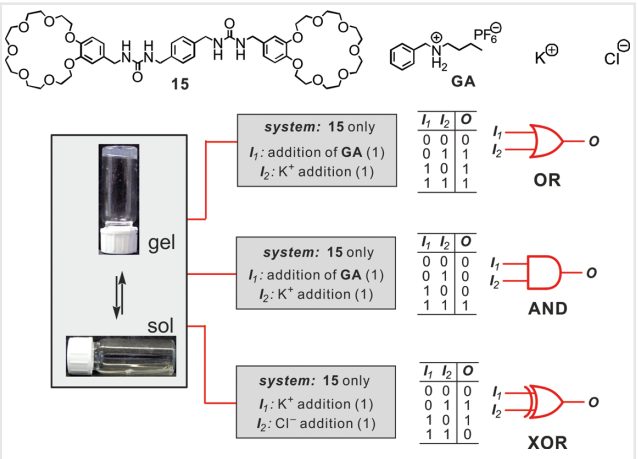

Figure 9 Molecular structure of gelator **15** and the logic gates (OR, AND, XOR) based on the sol–gel readouts after treating different stimuli. Adapted with permission from Ref. 85. Copyright 2012 The Royal Society of Chemistry.

of the gelator itself. In fact, they influence the self-assembly of the gelator, either to prohibit or to promote gelation. On the other side of the spectrum, stimuli that induce changes in the gelators can be exploited to switch between a gelator and a nongelator.

Recently, Ravoo and coworkers established versatile light-responsive gelators (**16**) based on a tripodal cyclohexane-1,3,5-tricarboxamide (CTA) core and three arylazopyrazole (AAP) arms (Scheme 6).[86] The CTA core provides face-to-face hydrogen bonding and a planar conformation, initiating the self-assembly of supramolecular polymers. AAP is a molecular photoswitch that isomerizes reversibly and reliably under alternating UV and green light irradiation with almost quantitative photoswitching.[87] The *E*-AAP is planar, favoring the self-assembly, whereas the *Z*-AAP has a twisted structure, leading to a disassembly of the supramolecular polymers. To improve the solubility of the gelators in water, a peptide sequence has been attached at the end of each arm. These hydrogelators are sensitive

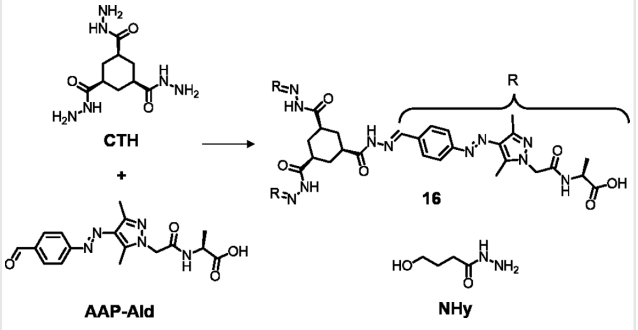

Scheme 6 Molecular structure of **16** and its in situ synthesis.

to pH, and in order to obtain homogenous hydrogels, GdL was applied to slowly generate an acidic environment due to its hydrolysis in water. Additionally, if a cyclohexanetrishydrazide (CTH) core is utilized, the hydrogelator and, hence, the hydrogel, forms in situ.[84] As a consequence, the hydrogel can be controlled by light and by dynamic covalent chemistry. A study of the light-responsive stiffness modulation demonstrates the additional π–π interactions from AAP moieties to be drastically diminished after UV irradiation due to the photoisomerization from the *E*- to the *Z*-state, so that the gel softened significantly. Upon green light irradiation, the π–π interactions are restored and thus the stiffness of the hydrogels is retrieved. The gelator's response to chemical stimuli has been investigated by adding a hydrazide competitor. When 4-hydroxybutyric acid hydrazide (NHy) is incorporated, the formation of the hydrogelator is suppressed, because NHy and CTH have equal probability to form hydrazones with the aldehyde (AAP-Ald), and a gel only forms at a sufficiently high concentration of **16**. At a lower NHy concentration (5 mM), formation of **16** is delayed. Yet, the thermodynamically stable **16** eventually wins out after 2 days. At a higher NHy concentration (25 mM), the formation of **16** is more or less suppressed so that the mixture remains liquid-like even after 5 days.

Multigelator Systems: Self-Sorting and Co-Assembly

If multiple gelator components are mixed, they can co-assemble in the same fibers or they can self-sort into different fibers of which each one contains only one gelator (Figure 10).[25,26] Both scenarios certainly have their benefits and drawbacks.

Self-Sorting

When two (or more) LMWGs have sufficiently different molecular structures and binding sites, the resulting gel is often composed of self-sorted supramolecular polymers. A pioneer example of self-sorting LMWGs was introduced by Shinkai and coworkers in 2008, in which self-sorted organogels with p–n heterojunction points were synthesized by mixing cholesteryl oligothiophenes and perylene.[88]

Recently, Adams and coworkers demonstrated a series of self-sorted hydrogels by making use of the intrinsic pK_a differences of the gelators (Figure 11).[89–91] For instance, the alanine-terminated perylene bisimide (PBI) **17** has two pK_a values of 6.6 and 5.4 and the phenylalanine-terminated stilbene **18** has a pK_a of 5.8.[90] The gelators are first dissolved at higher pH, followed by addition of GdL that hydrolyzes to generate an acidic environment. Usually, the gelator with

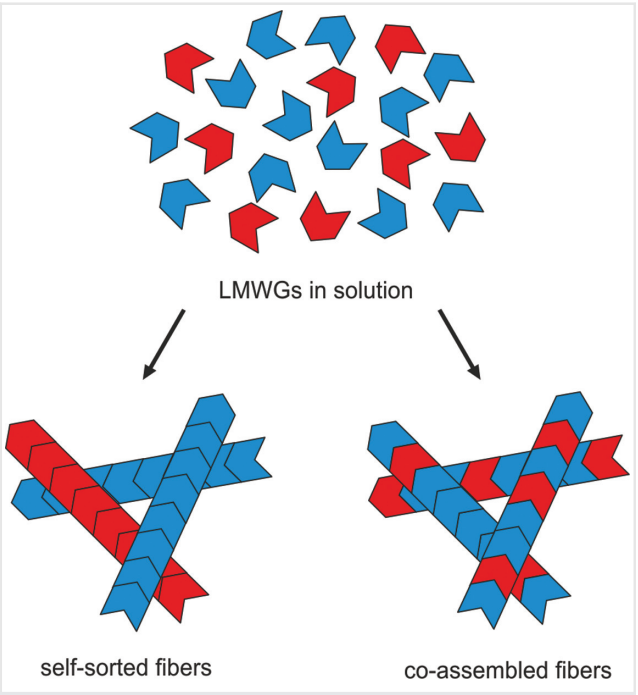

Figure 10 Self-assembly of multicomponent LMWGs, which can either self-sort into different fibers or co-assemble in the same fibers.

higher pK_a should self-assemble and form a gel first, when the pH slowly decreases. However, the authors observed that at the first pK_a of **17**, this gelator self-assembles into worm-like micelles and only forms a gel when the second pK_a (5.4) is reached. Consequently, the stilbene-based **18** forms fibers first, followed by PBI-based **17**, when the pH further decreases. This process can not only be monitored by NMR spectroscopy, in which the fibrous structure is inactive, but can also be demonstrated by rheological measurements. In addition, the UV absorption spectrum of gel-**17**,**18** is simply the superposition of the individual spectra of both gelators, suggesting a self-sorted network. Characterizing such multicomponent gels is often challenging.[92] The authors utilizes small-angle neutron scattering to support their hypothesis of self-sorting. Indeed, the self-sorted gel shows similar scattering as compared to that of the individual gels alone at different H_2O-to-D_2O ratios.[91] The presence of **18** nanofibers enables the formation of p–n heterojunctions, hence it shifts the irradiation wavelength from below 400 nm (**17** alone) to 420 nm.

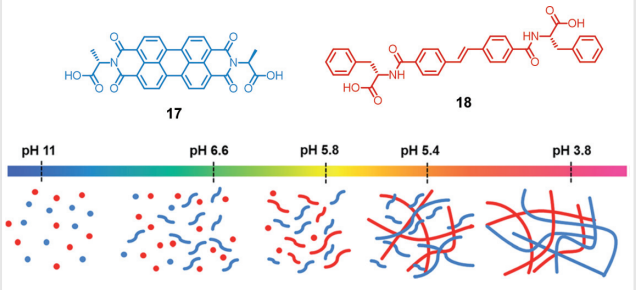

Figure 11 Molecular structures of the self-sorting building blocks **17** and **18** (top) Schematic representation of their stepwise self-assembly upon pH decrease (bottom). Adapted with permission from ref. 90. Copyright 2016 The Royal Society of Chemistry.

Thanks to the recent advances in microscopy techniques, a real-time imaging of supramolecular nanofibers becomes possible. Hamachi and coworkers exploited confocal laser scanning microscopy (CLSM) and stimulated emission depletion microscopy techniques to conceive a self-sorted network in a hydrogel.[93] Two gelators, **19** and **20**, and their fluorescent analogues (**19-F** and **20-F**) are mixed and treated with a heating–cooling cycle. The gelator pairs self-assemble orthogonally so that the green and red fibers do not overlap but instead entangled (Figure 12). CD spectra also support the self-sorting: a 1:1 mixture of **19** and **20** behaves just like the simple sum of the individual spectra. Lately, Hamachi's group investigated a postassembly fabrication protocol on the self-sorted hydrogel.[94] On one hand, Ca^{2+} ions interact with the phosphate groups of the nanofibers of **20**, so that the storage modulus (G') of the hybridized hydrogel increases by a factor of 4 (5.5 to 22.9 kPa). ATP addition leads to the capture of the Ca^{2+} ions and a softened gel ($G' = 8.6$ kPa). On the other hand, if sarcosine oxidase (SOx) is incorporated in the hybrid gel, the gel–sol transition takes place upon the addition of sarcosine, because SOx catalyzes the oxidative demethylation of sarcosine and produces H_2O_2, which decomposes aryl boronic acid-based gelators. In the end, an AND logic gate was devised based on the release of a fluorescein-labeled protein by treating the gel with ATP and sarcosine.

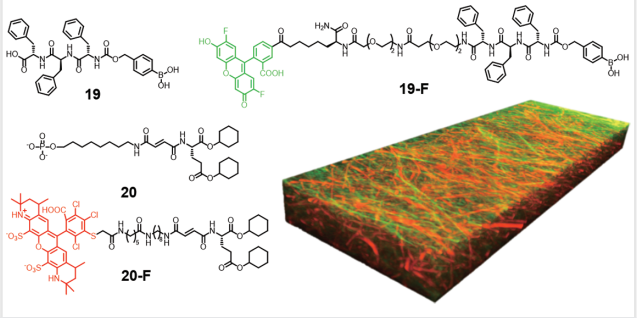

Figure 12 Molecular structures of the self-sorting building blocks **19** and **20**, and their corresponding fluorescent analogues **19-F** and **20-F**. Adapted with permission from Ref. 93. Copyright 2016 Nature Publishing Group.

Co-Assembly

In contrast to self-sorting systems, the molecular structures of the components in co-assembled gels are

usually quite alike.[95,96] One advantage of such supramolecular copolymers, compared to traditional copolymers, is that one could vary the functionality in the supramolecular copolymer by simply mixing different ratios of the main building block and its analogues.

Brito et al. established minimalistic proteoglycan mimics by co-assembling an aromatic dipeptide and carbohydrate amphiphiles (Figure 13).[97] The aromatic dipeptide amphiphile **21** dissolves in water at higher pH and self-assembles into nanotapes upon pH decrease. Due to the negatively charged groups in sulphate **22** or phosphate **23**, the carbohydrate amphiphiles self-assemble into micelles in water with negative zeta potentials of -112.0 ± 23.7 and -74.4 ± 5.3 mV, respectively. Co-assembly of the gelators (either **21**,**22** or **21**,**23**) is supported by spectroscopic and microscopic techniques. In CD experiments, a blue shift of the peak at 225 nm is observed (217 nm for **21**,**22** and 220 nm for **22**,**23**), suggesting changes in the superhelical structure caused by polarity changes upon the addition of carbohydrate amphiphiles. Instead, if the system is self-sorting, the peaks in CD experiments are simply the superposition of the individual peaks of both gelators. When **21** is mixed with the carbohydrate amphiphiles in a 2:1 ratio, the nanofibers are thickened compared to those assembled from pure **21** and have a negative zeta potential of ca. −55 mV in both the sulphate and the phosphate case. Moreover, not only the co-assembled supramolecular polymers form stiffer gels, but stiffness increases even more in the presence of Ca^{2+} ions, which may bridge the anions exposed on the fiber surface. These observations indicate that the carbohydrate amphiphiles are co-assembled with **21** as Fmoc groups act as stacking units, exposing the carbohydrates on the surface of the fibers. In the end, the authors demonstrated that the carbohydrate co-assembled hydrogels are noncytotoxic and can protect glycoprotein FGF-2 against degradation at 37 °C for 7 days.

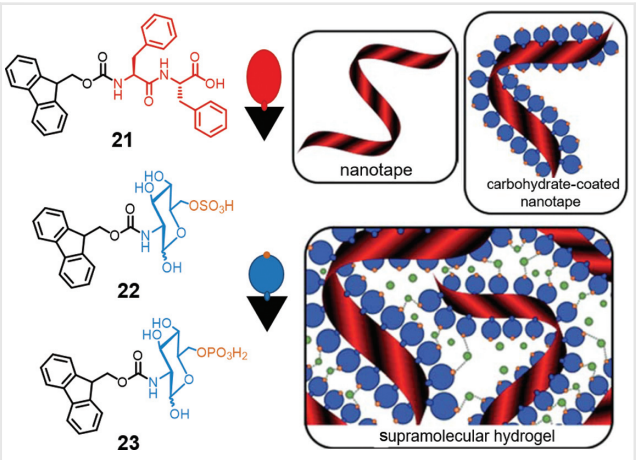

Figure 13 Molecular structures of co-assembled building blocks **21**, **22**, and **23** (left). Schematic representation of co-assembled carbohydrate supramolecular polymer and its hydrogel (right). Adapted with permission from Ref. 97. Copyright 2019 The Royal Society of Chemistry.

Ravoo and coworkers investigated a light-responsive co-assembled hydrogel using Fmoc-tetrapeptide **24** as the building block (Scheme 7).[98] Its peptide analogue **25** that contains the light-responsive AAP unit forms a co-assembled supramolecular polymer when mixed with **24.** To this system, cyclodextrin vesicles (CDVs) are added as additional cross-linking stations by using host–guest chemistry between AAP and β-cyclodextrin (β-CD). Since the photoisomerization of *E*- to *Z*-AAP correlates to intensely diminished binding affinity to β-CD, a light-responsive softening and stiffening of the peptide hydrogel is observed. The viscoelastic properties of the hydrogels examined by rheological measurements depend on the concentrations of both the peptide and CDV. Higher concentrations lead to higher degrees of cross-linking and thus stiffer materials. UV irradiation causes a decrease in storage modulus of 2 orders of magnitude. After green light irradiation, a more than 1 order of magnitude increase in stiffness is retrieved. Finally, photocontrolled release of multiple fluorescent payloads that were entrapped in the gel is detected. Upon UV irradiation, the hydrogel is softened and the payloads are released. Moreover, if the CDV is replaced by a magnetic nanoparticle-embedded CDV, the system could be controlled both by light and magnetic field.[99]

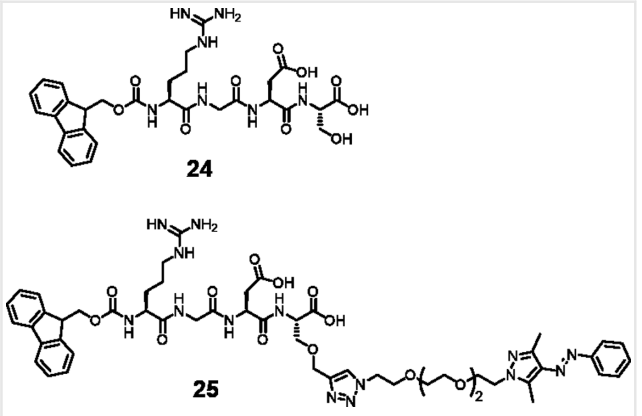

Scheme 7 Molecular structure of gelator **24** and its light-responsive analogue **25**.

Self-Sorting vs. Co-Assembly

The line along which self-sorting and co-assembly can be distinguished can sometimes be blurred. For instance,

Adams and coworkers compared the two-component gels of **26**,**27** and **26**,**28** under the same conditions (Scheme 8).[100]

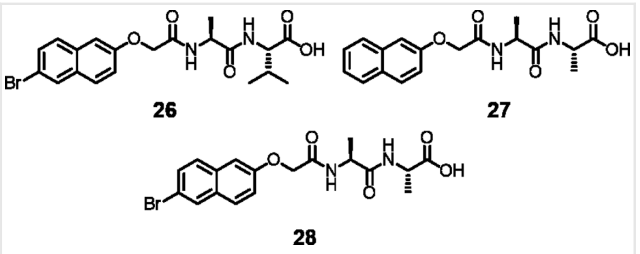

Scheme 8 Molecular structures of building blocks **26**, **27**, and **28** which either self-sort or co-assemble in the corresponding gels.

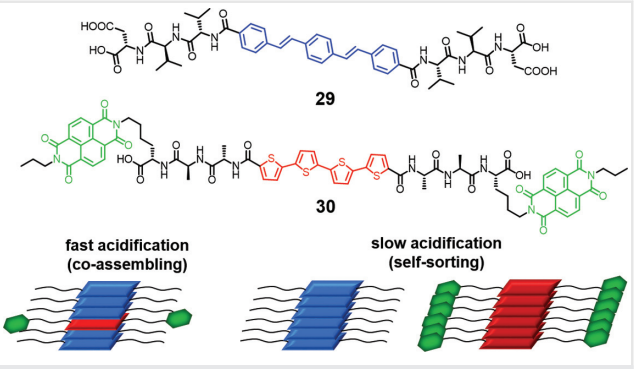

Figure 14 Molecular structures of gelators **29** and **30**. Their self-assembly is controlled by the acidification rates. Adapted with permission from Ref. 102. Copyright 2017 American Chemical Society.

At first glance, one may expect that the mixed gels should behave similarly because their molecular structures are quite alike. In fact, they act conversely. Gelators **26** and **27** have different C-terminal amino acids and thus different pK_a values. When these two gelators are dissolved at higher pH (ca. 10.5) followed by addition of GdL to slowly acidify the solution, self-sorted nanofibers are observed. In marked contrast, the gel formed from **26** and **28** is co-assembled from both gelators, although they have the same difference in the C-terminal amino acid. The authors attributed this difference to the co-assembled micelles formed from **26** and **28** already at higher pH. When monitoring the pH decrease, a plateau is found at a pH of 5.5, which is indeed between the individual pK_a values of **26** (5.9) and **28** (5.3). This observation supports the authors' hypothesis that co-assembled structures first form and then transform upon pH decrease into the final co-assembled gel. Yet, the mechanism is not completely clear. As another example, Escuder and coworkers demonstrated the importance of the molecular structures of gelators to obtain a co-assembled or self-sorted hydrogel that can perform catalysis.[101] A self-sorted network by a bolaamphiphilic gelator and an amphiphilic gelator can achieve one-pot deacetylation–aldol reactions, while a co-assembled network formed by two bolaamphiphilic gelators was shown to be catalytically inactive.

Not only a subtle change in molecular structure may result in distinctly different morphologies, but the kinetics of the self-assembly process can also have a great impact. Tovar and coworkers investigated self-sorted and randomly co-assembled two-component photoconductive gels, based on the same components, but strongly relying on the rate of acidification (Figure 14).[102] An electron-donating oligo(*p*-phenylenevinylene) peptide (**29**) and an electron-donor–acceptor peptide (**30**) based on quaterthiophene and naphthalene bisimide have been synthesized. Again, both **29** and **30** are dissolved at higher pH. When the system is acidified by GdL, the slow kinetics allow the gelators to experience the pH change. Due to their difference in pK_a (6.2 for **29** and 6.5 for **30**), the gelators start to self-assemble at different pH values, so that self-sorted gels are obtained. However, if the assembly is triggered by rapid addition of HCl, the gelators are unable to recognize the stepwise change in pK_a. Therefore, the co-assembled supramolecular polymers are obtained. The photophysical properties of self-sorted and co-assembled networks of **29** and **30** provide the following insights that (1) both exciton migration and resonance energy transfer are more efficient in the co-assembled system and (2) the self-sorted network is suitable for p–n heterojunctions.

Just recently, van Esch, Eelkema, and coworkers discovered a self-sorted system not only at a supramolecular, but also at a macroscopic level.[103,104] The gelators form in situ in a dynamic fashion by the reaction of trishydrazide (**H**) and neutral (**A**) or ionic aldehyde ($\mathbf{A}^-$). Hence, the resulting neutral or charged hydrazone gelators (NGs or CGs) simultaneously form hydrogels. HPLC experiments reveal both gelators to assemble at quite similar rates. However, the multicomponent gel encounters multilevel self-sorting, which is monitored by CLSM experiments. A fluorescein-labeled aldehyde (**A-FL**, green) is added to follow the self-assembly. In addition, the positively charged fluorophore Hoechst 33342 (blue) allows tracking specifically the growth of negatively charged fibers (CFs). When $\mathbf{A}^-$ reaches 15 mol%, crumbled sheets start to appear and a phase separation is observed (Figure 15a). The green fluorescence background is solely composed of bundles of neutral fibers (NFs). However, the wrinkled sheets are both green and blue fluorescence-active, suggesting the co-assembly of neutral and charged gelators and the development of CFs. The electrostatic repulsion of the CFs can effectively prevent themselves from bundling. In the time-dependent CLSM experiments, different nucleation rates of neutral and CFs are discovered. First, the NFs are self-assembled (green fluorescence), owing to their lower critical aggregation concentrations. After some time (stage 2), the CFs start to

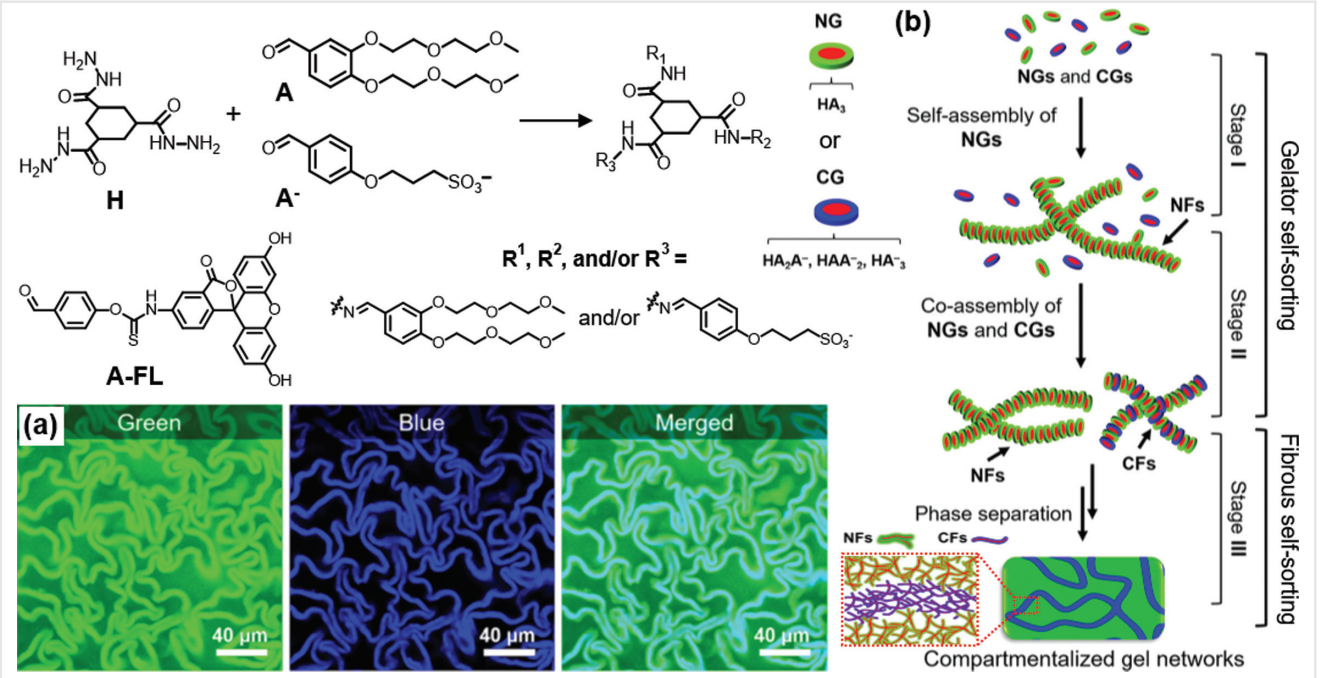

Figure 15 Molecular structures and the in situ synthesis of neutral and charged gelators. (a) CLSM images of macroscopic self-sorting. (b) Schematic illustration of the self-sorting process. A-FL and Hoechst 33342 were added for the visualization of green and blue fluorescence, respectively. Adapted and modified with permission from Ref. 103. Copyright 2019 American Chemical Society.

grow (by co-assembling of neutral and charged gelators) and homogenously mixed with NFs (homogeneous blue fluorescence). In the final step, the accumulated CFs lead to phase separation (blue wrinkled sheets and green coarse networks) (Figure 15b). Moreover, addition of NGs as seeds interferes with the nucleation rates of NGs and CGs and leads to homogenous, metastable gels.[104] The gels can later convert into the thermodynamically more stable states (wrinkled sheets) within a few weeks.

Conclusions and Outlook

In this review, we highlighted exemplarily advances in LMWGs made within the last decade and focused on stimuli-responsive gelators and multicomponent systems that undergo self-sorting and/or co-assembly. In contrast to earlier reviews on stimuli-responsive gelators,[23,27] we discussed the stimuli from a different perspective by categorizing them into effects on the bulk solution or on the gelators.

Within the last decade, we have also witnessed great progress in the development of sophisticated energy-driven systems which operate out of the thermodynamic equilibrium and thus exhibit interesting emergent properties such as transient gelation processes. The employment of multi-stimuli responsive gelators paves the ways to functional materials, such as logic gates and biosensors. The work dedicated to multicomponent gels even with stepwise control over their self-assembly will certainly have a strong impact on the development of more complex LMWG systems. Furthermore, with recent advances in microscopy techniques, such multicomponent systems, can be more accurately characterized. The possibility of observing the growth of nanofibers in real time helps us understand the mechanism of the gelling process.

The field of supramolecular gels is currently in the transition process from serendipitously discovering gelators to deliberately and systematically designing them. Still, surprising results are frequent. For instance, a small variation of a known gelator often changes the whole game.[100] This is often attributed to their nucleation and gelation processes under different circumstances. Explicit methodologies for studying the mechanisms are yet to be developed and refined.

What may we expect in the next decade? As we observe in the latest decade, the attention of LMWGs moves from organo towards hydrogels for the sake of biomedical applications. Compared to the search for covalent biodegradable polymers, supramolecular hydrogels can more easily be degraded by the body as they are reversibly built from small molecules. Employing stimuli-responsive supramolecular gels for biomedical applications has shown promising progress. For example, a reversible yet robust hydrogel assembled from DNA–peptide conjugates that organize into intertwined filaments has shown reversibly tunable storage moduli as the superstructures are

disassembled upon changes in charge density.[105] Also, using a fluorophore-containing conjugate for monitoring enzyme-catalyzed self-assembly of peptides inside living cells has been demonstrated, providing us with insightful information for the future design of LMWGs.[106]

Designing a hydrogelator is challenging as the strength of hydrogen bonds, a common driving force for organogelators to form aggregates, is largely diminished in aqueous solution. Instead, hydrophobic interactions become a key driving force and to control them becomes critical. A balance between the tendency of molecules to dissolve or to aggregate must be reached to achieve gelation. Although there is certainly progress in biocompatible LMWGs, a gap in function between natural and synthetic supramolecular systems still remains. To bridge this gap, we may expect progresses in dissipative systems as living systems dissipate energy to stay far from thermodynamic equilibrium. Fuel-driven gels enable the development of systems that consume energy to perform functions autonomously. Also, improving the robustness of the gels from LMWGs becomes crucial, if we aim at replacing polymeric materials with fully reversible, recyclable, supramolecular materials.

Acknowledgment

We acknowledge Deutsche Forschungsgemeinschaft for continuous financial support to our work.

References

(1) Estroff, L. A.; Hamilton, A. D. *Chem. Rev.* **2004**, *104*, 1201.
(2) Terech, P.; Weiss, R. G. *Chem. Rev.* **1997**, *97*, 3133.
(3) Chen, L.; Tian, Y. K.; Ding, Y.; Tian, Y. J.; Wang, F. *Macromolecules* **2012**, *45*, 8412.
(4) Liu, D.; Wang, D.; Wang, M.; Zheng, Y.; Koynov, K.; Auernhammer, G. K.; Butt, H.-J.; Ikeda, T. *Macromolecules* **2013**, *46*, 4617.
(5) Harada, A.; Takashima, Y.; Nakahata, M. *Acc. Chem. Res.* **2014**, *47*, 2128.
(6) Rodell, C. B.; MacArthur, J. W.; Dorsey, S. M.; Wade, R. J.; Wang, L. L.; Woo, Y. J.; Burdick, J. A. *Adv. Funct. Mater.* **2015**, *25*, 636.
(7) Appel, E. A.; Loh, X. J.; Jones, S. T.; Biedermann, F.; Dreiss, C. A.; Scherman, O. A. *J. Am. Chem. Soc.* **2012**, *134*, 11767.
(8) Park, K. M.; Yang, J. A.; Jung, H.; Yeom, J.; Park, J. S.; Park, K. H.; Hoffman, A. S.; Hahn, S. K.; Kim, K. *ACS Nano* **2012**, *6*, 2960.
(9) Wang, Q.; Mynar, J. L.; Yoshida, M.; Lee, E.; Lee, M.; Okuro, K.; Kinbara, K.; Aida, T. *Nature* **2010**, *463*, 339.
(10) Hunt, J. N.; Feldman, K. E.; Lynd, N. A.; Deek, J.; Campos, L. M.; Spruell, J. M.; Hernandez, B. M.; Kramer, E. J.; Hawker, C. J. *Adv. Mater.* **2011**, *23*, 2327.
(11) Raeburn, J.; Zamith Cardoso, A.; Adams, D. J. *Chem. Soc. Rev.* **2013**, *42*, 5143.
(12) Mattia, E.; Otto, S. *Nat. Nanotechnol.* **2015**, *10*, 111.
(13) van Esch, J. H. *Langmuir* **2009**, *25*, 8392.
(14) de Loos, M.; Feringa, B. L.; van Esch, J. H. *Eur. J. Org. Chem.* **2005**, 3615.
(15) van Esch, J. H.; Feringa, B. L. *Angew. Chem. Int. Ed.* **2000**, *39*, 2263.
(16) Weiss, R. G. *J. Am. Chem. Soc.* **2014**, *136*, 7519.
(17) Okesola, B. O.; Smith, D. K. *Chem. Soc. Rev.* **2016**, *45*, 4226.
(18) Amabilino, D. B.; Smith, D. K.; Steed, J. W. *Chem. Soc. Rev.* **2017**, *46*, 2404.
(19) Fleming, S.; Ulijn, R. V. *Chem. Soc. Rev.* **2014**, *43*, 8150.
(20) Tao, K.; Levin, A.; Adler-Abramovich, L.; Gazit, E. *Chem. Soc. Rev.* **2016**, *45*, 3935.
(21) Tam, A. Y. Y.; Yam, V. W. W. *Chem. Soc. Rev.* **2013**, *42*, 1540.
(22) Piepenbrock, M.-O. M.; Lloyd, G. O.; Clarke, N.; Steed, J. W. *Chem. Rev.* **2010**, *110*, 1960.
(23) Jones, C. D.; Steed, J. W. *Chem. Soc. Rev.* **2016**, *45*, 6546.
(24) Draper, E. R.; Adams, D. J. *Chem. Commun.* **2016**, *52*, 8196.
(25) Buerkle, L. E.; Rowan, S. J. *Chem. Soc. Rev.* **2012**, *41*, 6089.
(26) Raeburn, J.; Adams, D. J. *Chem. Commun.* **2015**, *51*, 5170.
(27) Offiler, C. A.; Jones, C. D.; Steed, J. W. *Chem. Commun.* **2017**, *53*, 2024.
(28) Laurence, C.; Berthelot, M. *Perspect. Drug Discovery Des.* **2000**, *18*, 39.
(29) Lloyd, G. O.; Piepenbrock, M.-O. M.; Foster, J. A.; Clarke, N.; Steed, J. W. *Soft Matter* **2012**, *8*, 204.
(30) Lo Nostro, P.; Ninham, B. W. *Chem. Rev.* **2012**, *112*, 2286.
(31) Jaspers, M.; Rowan, A. E.; Kouwer, P. H. J. *Adv. Funct. Mater.* **2015**, *25*, 6503.
(32) Roy, S.; Javid, N.; Frederix, P. W. J. M.; Lamprou, D. A.; Urquhart, A. J.; Hunt, N. T.; Halling, P. J.; Ulijn, R. V. *Chem. Eur. J.* **2012**, *18*, 11723.
(33) Pang, Z.; Wei, Y.; Wang, N.; Zhang, J.; Gao, Y.; Qian, S. *Int. J. Pharm.* **2018**, *548*, 625.
(34) Fuentes-Caparrós, A. M.; de Paula Gómez-Franco, F.; Dietrich, B.; Wilson, C.; Brasnett, C.; Seddon, A.; Adams, D. J. *Nanoscale* **2019**, *11*, 3275.
(35) Yan, M.; Velu, S. K. P.; Maréchal, M.; Royal, G.; Galvez, J.; Terech, P. *Soft Matter* **2013**, *9*, 4428.
(36) Kuroiwa, K.; Shibata, T.; Takada, A.; Nemoto, N.; Kimizuka, N. *J. Am. Chem. Soc.* **2004**, *126*, 2016.
(37) de Hatten, X.; Bell, N.; Yufa, N.; Christmann, G.; Nitschke, J. R. *J. Am. Chem. Soc.* **2011**, *133*, 3158.
(38) Asil, D.; Foster, J. A.; Patra, A.; de Hatten, X.; del Barrio, J.; Scherman, O. A.; Nitschke, J. R.; Friend, R. H. *Angew. Chem. Int. Ed.* **2014**, *53*, 8388.
(39) Nebot, V. J.; Ojeda-Flores, J. J.; Smets, J.; Fernández-Prieto, S.; Escuder, B.; Miravet, J. F. *Chem. Eur. J.* **2014**, *20*, 14465.
(40) Michnik, A.; Sułkowska, A. *J. Mol. Struct.* **1997**, *410*, 17.
(41) Cravotto, G.; Cintas, P. *Chem. Soc. Rev.* **2006**, *35*, 180.
(42) Baig, R. B. N.; Varma, R. S. *Chem. Soc. Rev.* **2012**, *41*, 1559.
(43) Cravotto, G.; Cintas, P. *Chem. Soc. Rev.* **2009**, *38*, 2684.
(44) Naota, T.; Koori, H. *J. Am. Chem. Soc.* **2005**, *127*, 9324.
(45) Komiya, N.; Muraoka, T.; Iida, M.; Miyanaga, M.; Takahashi, K.; Naota, T. *J. Am. Chem. Soc.* **2011**, *133*, 16054.
(46) Naito, M.; Inoue, R.; Iida, M.; Kuwajima, Y.; Kawamorita, S.; Komiya, N.; Naota, T. *Chem. Eur. J.* **2015**, *21*, 12927.
(47) Yu, X.; Chen, L.; Zhang, M.; Yi, T. *Chem. Soc. Rev.* **2014**, *43*, 5346.
(48) Pappas, C. G.; Frederix, P. W. J. M.; Mutasa, T.; Fleming, S.; Abul-Haija, Y. M.; Kelly, S. M.; Gachagan, A.; Kalafatovic, D.; Trevino, J.; Ulijn, R. V.; Bai, S. *Chem. Commun.* **2015**, *51*, 8465.
(49) Pappas, C. G.; Mutasa, T.; Frederix, P. W. J. M.; Fleming, S.; Bai, S.; Debnath, S.; Kelly, S. M.; Gachagan, A.; Ulijn, R. V. *Mater. Horiz.* **2015**, *2*, 198.

(50) Núñez-Villanueva, D.; Jinks, M. A.; Gómez Magenti, J.; Hunter, C. A. *Chem. Commun.* **2018**, *54*, 10874.
(51) Sui, X.; Feng, X.; Hempenius, M. A.; Vancso, G. J. *J. Mater. Chem. B* **2013**, *1*, 1658.
(52) van Staveren, D. R.; Metzler-Nolte, N. *Chem. Rev.* **2004**, *104*, 5931.
(53) Martić, S.; Labib, M.; Shipman, P. O.; Kraatz, H.-B. *Dalton Trans.* **2011**, *40*, 7264.
(54) Adhikari, B.; Kraatz, H.-B. *Chem. Commun.* **2014**, *50*, 5551.
(55) Bendikov, M.; Wudl, F.; Perepichka, D. F. *Chem. Rev.* **2004**, *104*, 4891.
(56) Schröder, H. V.; Schalley, C. A. *Beilstein J. Org. Chem.* **2018**, *14*, 2163.
(57) Nalluri, S. K. M.; Shivarova, N.; Kanibolotsky, A. L.; Zelzer, M.; Gupta, S.; Frederix, P. W. J. M.; Skabara, P. J.; Gleskova, H.; Ulijn, R. V. *Langmuir* **2014**, *30*, 12429.
(58) Murata, K.; Aoki, M.; Suzuki, T.; Harada, T.; Kawabata, H.; Komori, T.; Ofaseto, F.; Ueda, K.; Shinkai, S. *J. Am. Chem. Soc.* **1994**, *116*, 6664.
(59) Yang, R.; Peng, S.; Hughes, T. C. *Soft Matter* **2014**, *10*, 2188.
(60) Fatás, P.; Bachl, J.; Oehm, S.; Jiménez, A. I.; Cativiela, C.; Díaz Díaz, D. *Chem. Eur. J.* **2013**, *19*, 8861.
(61) Sahoo, J. K.; Nalluri, S. K. M.; Javid, N.; Webb, H.; Ulijn, R. V. *Chem. Commun.* **2014**, *50*, 5462.
(62) Irie, M. *Chem. Rev.* **2000**, *100*, 1685.
(63) Irie, M.; Fukaminato, T.; Matsuda, K.; Kobatake, S. *Chem. Rev.* **2014**, *114*, 12174.
(64) van Herpt, J. T.; Stuart, M. C. A.; Browne, W. R.; Feringa, B. L. *Chem. Eur. J.* **2014**, *20*, 3077.
(65) Kelly, T. R.; De Silva, H.; Silva, R. A. *Nature* **1999**, *401*, 150.
(66) Koumura, N.; Zijlstra, R. W.; van Delden, R. A.; Harada, N.; Feringa, B. L. *Nature* **1999**, *401*, 152.
(67) Koumura, N.; Geertsema, E. M.; van Gelder, M. B.; Meetsma, A.; Feringa, B. L. *J. Am. Chem. Soc.* **2002**, *124*, 5037.
(68) Chen, J.; Leung, F. K.-C.; Stuart, M. C. A.; Kajitani, T.; Fukushima, T.; van der Giessen, E.; Feringa, B. L. *Nat. Chem.* **2018**, *10*, 132.
(69) Iwaso, K.; Takashima, Y.; Harada, A. *Nat. Chem.* **2016**, *8*, 625.
(70) van Rossum, S. A. P.; Tena-Solsona, M.; van Esch, J. H.; Eelkema, R.; Boekhoven, J. *Chem. Soc. Rev.* **2017**, *46*, 5519.
(71) De, S.; Klajn, R. *Adv. Mater.* **2018**, *30*, 1706750.
(72) Adams, D. J.; Butler, M. F.; Frith, W. J.; Kirkland, M.; Mullen, L.; Sanderson, P. *Soft Matter* **2009**, *5*, 1856.
(73) Heuser, T.; Weyandt, E.; Walther, A. *Angew. Chem. Int. Ed.* **2015**, *54*, 13258.
(74) Panja, S.; Patterson, C.; Adams, D. J. *Macromol. Rapid Commun.* **2019**, *40*, 1900251.
(75) Debnath, S.; Roy, S.; Ulijn, R. V. *J. Am. Chem. Soc.* **2013**, *135*, 16789.
(76) Pappas, C. G.; Sasselli, I. R.; Ulijn, R. V. *Angew. Chem. Int. Ed.* **2015**, *54*, 8119.
(77) Oka, T.; Morihara, K. *J. Biochem.* **1977**, *82*, 1055.
(78) Fastrez, J.; Fersht, A. R. *Biochemistry* **1973**, *12*, 2025.
(79) Boekhoven, J.; Brizard, A. M.; Kowlgi, K. N. K.; Koper, G. J. M.; Eelkema, R.; van Esch, J. H. *Angew. Chem. Int. Ed.* **2010**, *49*, 4825.
(80) Boekhoven, J.; Hendriksen, W. E.; Koper, G. J. M.; Eelkema, R.; van Esch, J. H. *Science* **2015**, *349*, 1075.
(81) Versluis, F.; van Elsland, D. M.; Mytnyk, S.; Perrier, D. L.; Trausel, F.; Poolman, J. M.; Maity, C. *J. Am. Chem. Soc.* **2016**, *138*, 8670.
(82) Trausel, F.; Versluis, F.; Maity, C.; Poolman, J. M.; Lovrak, M.; van Esch, J. H.; Eelkema, R. *Acc. Chem. Res.* **2016**, *49*, 1440.
(83) Olive, A. G. L.; Abdullah, N. H.; Ziemecka, I.; Mendes, E.; Eelkema, R.; van Esch, J. H. *Angew. Chem. Int. Ed.* **2014**, *53*, 4132.
(84) Boekhoven, J.; Poolman, J. M.; Maity, C.; Li, F.; van der Mee, L.; Minkenberg, C. B.; Mendes, E.; van Esch, J. H.; Eelkema, R. *Nat. Chem.* **2013**, *5*, 433.
(85) Qi, Z.; Malo de Molina, P.; Jiang, W.; Wang, Q.; Nowosinski, K.; Schulz, A.; Gradzielski, M.; Schalley, C. A. *Chem. Sci.* **2012**, *3*, 2073.
(86) Chu, C.-W.; Stricker, L.; Kirse, T. M.; Hayduk, M.; Ravoo, B. J. *Chem. Eur. J.* **2019**, *25*, 6131.
(87) Weston, C. E.; Richardson, R. D.; Haycock, P. R.; White, A. J. P.; Fuchter, M. J. *J. Am. Chem. Soc.* **2014**, *136*, 11878.
(88) Sugiyasu, K.; Kawano, S.-I.; Fujita, N.; Shinkai, S. *Chem. Mater.* **2008**, *20*, 2863.
(89) Draper, E. R.; Eden, E. G. B.; McDonald, T. O.; Adams, D. J. *Nat. Chem.* **2015**, *7*, 848.
(90) Draper, E. R.; Lee, J. R.; Wallace, M.; Jäckel, F.; Cowan, A. J.; Adams, D. J. *Chem. Sci.* **2016**, *7*, 6499.
(91) Cross, E. R.; Sproules, S.; Schweins, R.; Draper, E. R.; Adams, D. J. *J. Am. Chem. Soc.* **2018**, *140*, 8667.
(92) Draper, E. R.; Adams, D. J. *Chem. Soc. Rev.* **2018**, *47*, 3395.
(93) Onogi, S.; Shigemitsu, H.; Yoshii, T.; Tanida, T.; Ikeda, M.; Kubota, R.; Hamachi, I. *Nat. Chem.* **2016**, *8*, 743.
(94) Tanaka, W.; Shigemitsu, H.; Fujisaku, T.; Kubota, R.; Minami, S.; Urayama, K.; Hamachi, I. *J. Am. Chem. Soc.* **2019**, *141*, 4997.
(95) Brunsveld, L.; Folmer, B. J. B.; Meijer, E. W.; Sijbesma, R. P. *Chem. Rev.* **2001**, *101*, 4071.
(96) Aida, T.; Meijer, E. W.; Stupp, S. I. *Science* **2012**, *335*, 813.
(97) Brito, A.; Abul-Haija, Y. M.; da Costa, D. S.; Novoa-Carballal, R.; Reis, R. L.; Ulijn, R. V.; Pires, R. A.; Pashkuleva, I. *Chem. Sci.* **2019**, *10*, 2385.
(98) Chu, C.-W.; Ravoo, B. J. *Chem. Commun.* **2017**, *53*, 12450.
(99) Nowak, B. P.; Ravoo, B. J. *Faraday Discuss.* **2019**, *219*, 220.
(100) Colquhoun, C.; Draper, E. R.; Eden, E. G. B.; Cattoz, B. N.; Morris, K. L.; Chen, L.; McDonald, T. O.; Terry, A. E.; Griffiths, P. C.; Serpell, L. C.; Adams, D. J. *Nanoscale* **2014**, *6*, 13719.
(101) Singh, N.; Zhang, K.; Angulo-Pachón, C. A.; Mendes, E.; van Esch, J. H.; Escuder, B. *Chem. Sci.* **2016**, *7*, 5568.
(102) Ardoña, H. A. M.; Draper, E. R.; Citossi, F.; Wallace, M.; Serpell, L. C.; Adams, D. J.; Tovar, J. D. *J. Am. Chem. Soc.* **2017**, *139*, 8685.
(103) Wang, Y.; Lovrak, M.; Liu, Q.; Maity, C.; le Sage, V. A. A.; Guo, X.; Eelkema, R.; van Esch, J. H. *J. Am. Chem. Soc.* **2019**, *141*, 2847.
(104) Wang, Y.; de Kruijff, R. M.; Lovrak, M.; Guo, X.; Eelkema, R.; van Esch, J. H. *Angew. Chem. Int. Ed.* **2019**, *58*, 3800.
(105) Freeman, R.; Han, M.; Álvarez, Z.; Lewis, J. A.; Wester, J. R.; Stephanopoulos, N.; McClendon, M. T.; Lynsky, C.; Godbe, J. M.; Sangji, H.; Luijten, E.; Stupp, S. I. *Science* **2018**, *362*, 808.
(106) Gao, Y.; Shi, J.; Yuan, D.; Xu, B. *Nat. Commun.* **2012**, *3*, 1033.